

AUTO-COMBUSTION FACILE SYNTHESIS AND PHOTOCATALYTIC HYDROGEN EVOLUTION ACTIVITY OF Al AND Ni CO-DOPED ZnO NANOPARTICLES

I. AHMAD^a, M. E. MAZHAR^a, M. N. USMANI^{a,*}, K. KHAN^b, S. AHMAD^c, J. AHMAD^a

^a*Department of Physics, BahauddinZakariya University, Multan. Pakistan*

^b*Department of Electrical Engineering, The University of Azad Jammu and Kashmir, Pakistan*

^c*Department of Building and Architectural Engineering, UCE&T, BahauddinZakariya University, Multan. Pakistan*

Aluminium (Al) and nickel (Ni) co-doped ZnO nanoparticles were synthesized by facile auto-combustion method and followed by calcinations at 700°C for 3hours. The prepared nanoparticles were characterized by X-ray diffraction (XRD), scanning electron microscopy (SEM), Raman spectroscopy, UV-vis diffuse reflectance spectroscopy (UV-vis DRS), and photoluminescence spectroscopy (PL) techniques. The XRD pattern of Al, Ni co-doped ZnO nanoparticles was found to be hexagonal and clarified the co-existence of Al and Ni into ZnO by peaks shift towards lower 2θ values. The crystal growth mechanism was successfully suppressed due to Al and Ni doping, confirmed by XRD results. Nearly spherical morphology of prepared samples was confirmed by SEM results. The absorption spectra indicated that optical band gap energy for Al, Ni co-doped ZnO nanoparticles was in range of 3.30-3.27 eV. The band gap energy decreased for low doping concentration and then increased for higher doping concentrations of Al, Ni. The photocatalytic performance of prepared samples was measured in 90 mL aqueous solution containing 15 mL lactic acid (LA) under visible light irradiation and (x=3%) sample showed highest photocatalytic performance for hydrogen evolution ($5.68 \text{ mmol}\cdot\text{h}^{-1}\cdot\text{g}^{-1}$) as compared to ($0.24 \text{ mmol}\cdot\text{h}^{-1}\cdot\text{g}^{-1}$) for pure ZnO. This useful result of improved photocatalytic performance was attributed to increased absorption of visible light and minimum electron hole pair rate.

(Received September 30, 2018; Accepted January 3, 2019)

Keywords: Co-doped Nanoparticles, Auto-combustion facile synthesis, Photocatalytic performance, Raman spectroscopy

1. Introduction

Every day, many organic pollutants are discharged into water from industries. Reports tell that textile industry uses about 10,000 pigments and dyes. The basic need of life on earth is clean water and it is becoming pollutant day by day due to development of dyestuffs by industrial textile. Semiconductor photocatalysts have been used for degradation of their stable chemical structure due to facile synthesis, small energy utilization and smooth reaction conditions under ultraviolet light irradiation [1-2]. Due to costly and tough implementation of UV light source, naturally rich existing sunlight renewable energy source is used for photo sensitizer excitation to react with molecular oxygen to produce superoxide radical anions and hydroxyl radicals, which degrade organic pollutants.

Metal oxide semiconductor nanomaterials are considered to be of great importance due to intensive applications in environmental remediation, LEDs, gas sensing, UV photo detector, solar cells, microelectronics and biomedicine etc [3-6]. One dimensional photocatalysts have exhibited good performance among nano scaled materials. Size and shape largely influence the properties of

*Corresponding author: naumanusmani@bzu.edu.pk

these nano materials [7-8], and nano materials with different shapes such as nanobelts and nanowires [9-10], nanospheres [11], nanoplates [12] and nanoflowers [13] are prepared.

ZnO nanoparticles photocatalysts have attracted huge attention due to their stability, strong oxidizing power, wide band gap, non-toxicity, low cost price [14-18], large photocatalytic performance and less energy utilization [19-22]. ZnO is an n-type II-VI subgroup semiconductor possessing crystalline wurtzite structure and wide band gap of 3.37 eV [23]. ZnO has been used in substitution to TiO₂ photocatalyst due to its large absorption ability in short wavelength of solar spectrum and high quantum efficiency [23-25].

Photocatalytic performance of ZnO is hindered due to its wide band gap, quick electron hole pair rate, poor adsorption ability, limited reusability and minute photocatalytic efficiency to visible range of solar spectrum, despite of being a highly active photocatalyst [26]. Photocatalytic performance of ZnO is largely affected by fast electron hole pair rate and lower interfacial charge carrier transfer rate. Several ways have been used to reduce electron hole pair rate and to enhance interfacial charge carrier transfer rate like physical modification as morphology [27], introducing surface defects and doping with non-metals and transition metals [28-30].

Therefore, photocatalytic efficiency is made better in visible range of solar spectrum with doping of transition metals impurities (Al, Ag, Cu, Ni, Co etc) for large absorption in visible range [31-37]. The properties of ZnO are changed by incorporation of transition metals ions into crystal lattice of ZnO, due to which absorption is shifted to visible spectrum and band gap is lowered [23].

The impact of Al dopants on photocatalytic performances of ZnO is investigated extensively due to its low cost price and large abundance in earth [38-39]. Lee et al [35] prepared Al doped ZnO nanoparticles for hydrogen production with different Al doping concentration by precipitation method. The best photocatalytic performance under visible light irradiation was shown by 3 mol% Al doped ZnO sample for degradation of methyl orange due to low electron hole pair rate. Ahmad et al [41] synthesized Al doped ZnO nanoparticles by a facile auto-combustion method with different Al concentration. The band gap was reduced from 3.21 eV for pure ZnO to 3.12 eV for 6 mol% Al doped ZnO nanoparticles. The catalytic efficiency was observed by methyl orange (MO) photo degradation and best result was shown by 4 mol% Al doped ZnO nanoparticles with 100% photo degradation while pure ZnO showed only 23% degradation after 1.5h irradiation.

Ni doping also improved photocatalytic performance of ZnO by enhancing visible light absorption due to creation of impurity levels in band gap and thus reducing electron hole pair rate [42-43]. Zhao et al [44] synthesized nickel doped ZnO nanorods for photocatalytic applications by degradation of rhodamine B (RB) under solar light irradiation. Brick et al [45] synthesized Ni doped ZnO samples and studied photocatalytic efficiency. The results showed that Ni doped ZnO had much higher photocatalytic efficiency than pure ZnO for degradation of methyl orange blue. In his work, reported morphology of photocatalyst was spherical aggregation with size of about 1 μ m.

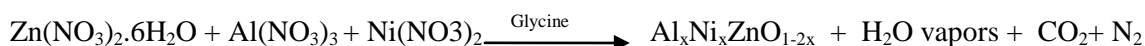
Currently, a lot of research is being done on co-doping semiconductor photocatalyst due to its higher performance and unique properties as compared to a single doped semiconductor photocatalyst. Existing literature reports that co-doped metal photocatalyst such as Zn-Ag ZnO [89] and Ce-Ag ZnO [46] show excellent photocatalytic activity for degradation of poisonous dyes and pigments as compared to single doped photocatalyst. Cd and Al [47], Pd and N [48], Ag and V [49] and Ga, Al, Co [50] doped semiconductor photocatalyst have been studied. The motivation of present research work is the preparation of Al loaded Ni-ZnO nanoparticles for hydrogen production by facile auto-combustion method to investigate photocatalytic performance.

2. Experimental

2.1. Preparation

A facile auto-combustion method was used to prepare Al, Ni co-doped ZnO nanoparticles Al_xNi_xZnO_{1-2x} (x= 0%, 1%, 2%, 3%, 4%, 5%) using Zinc nitrate Zn(NO₃)₂·6H₂O, Aluminium nitrate Al(NO₃)₃, nickel nitrate Ni(NO₃)₂ and glycine NH₂CH₂COOH from Aldrich company, as starting materials. Glycine was used as a fuel for combustion reaction. Chemicals in required

amount were mixed and placed in open atmosphere to absorb moisture. The mixture underwent through heat treatment along with stirring for 1h at 90°C-100°C to attain homogeneity. The color of homogeneous mixture changed from white yellow to yellow and finally turned to blackish gel. The gel precursors were further stirred at temperature range 170 °C-210°C. The gel was swelled into foam like material following self-combustion reaction. Synthesized powder was collected and calcined at 700°C for 3h to obtain fine nanoparticles.



2.2. Characterization

The crystalline structure of prepared $\text{Al}_x\text{Ni}_x\text{ZnO}_{1-2x}$ nanoparticles was investigated by Xpert PRO XRD diffractometer (CuK α radiation $\lambda=1.5406 \text{ \AA}$) at 30kV voltage and 20mA current in 2θ range of 20°-80° with step width of 0.02°. The surface morphology was explored by SEM using a JSM-6701F-6701 instrument. The optical properties of synthesized $\text{Al}_x\text{Ni}_x\text{ZnO}_{1-2x}$ nanoparticles were examined with Perkin-Elmer LS 55 fluorescence spectrometer in 320-600 nm range at room temperature. DRS were calculated with Shimadzu UV-2450 instrument. Raman spectra were calculated with BWTeki-i-micro plus system with 5x magnification lens and nearly 3cm^{-1} accuracy in Raman shift.

3. Results and discussions

3.1 XRD

The XRD patterns employed to study the changes in phase structure and crystal size of prepared pure ZnO and $\text{Al}_x\text{Ni}_x\text{ZnO}_{1-2x}$ nanoparticles are shown in figure 1. XRD patterns of ZnO nanoparticles clearly show that diffraction peaks have strong intensity, sharpness and narrow width, which is an indication of good crystallinity. However intensity slightly lowers with increase in Al, Ni doping concentration. This indicates that Al and Ni doping reduces crystallinity and particles size of $\text{Al}_x\text{Ni}_x\text{ZnO}_{1-2x}$ nanoparticles [51]. The major diffraction peaks of pure ZnO were indexed with standard hexagonal phase wurtzite ZnO which are in good agreement with JCPDS No 35-1415 and previous studies [52,53]. The diffraction peaks observed at 2θ values of 31.78°, 36.28°, 38.23°, 48.52°, 56.71°, 62.85°, 66.53°, 67.95°, 69.16° and 76.96° correspond to (100), (002), (101), (102), (110), (103), (200), (112), (201) and (202) planes of wurtzite ZnO. No other diffraction peaks were observed for pure ZnO. The diffraction pattern for $\text{Al}_x\text{Ni}_x\text{ZnO}_{1-2x}$ nanoparticles was different from pure ZnO.

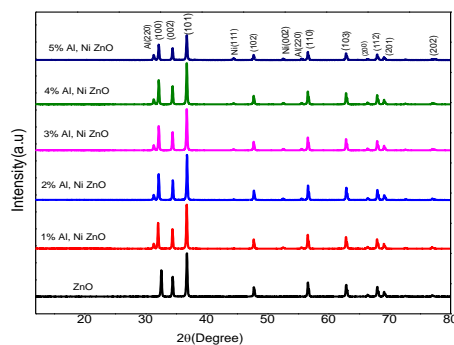


Fig. 1. XRD patterns of ZnO and $\text{Al}_x\text{Ni}_x\text{ZnO}_{1-2x}$ nanoparticles.

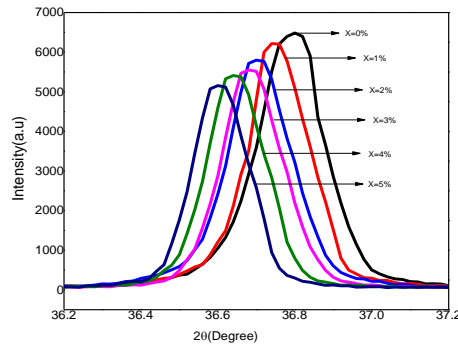


Fig. 2. Enlarged diffraction spectra of $Al_xNi_xZnO_{1-2x}$ nanoparticles from 36.2° to 37.2° along (101) plane.

Fig.2 shows peak positions shifted slightly towards smaller 2θ values for Al, Ni co-doped ZnO samples as compared to pure ZnO sample. This peak shift may be attributed to ionic radii difference of $Al^{+2}(0.54\text{\AA})$ and $Ni^{+2}(0.69\text{\AA})$ compared to that of $Zn^{+2}(0.74\text{\AA})$ [54]. This result confirms that Al and Ni had been successfully substituted into ZnO sites. Also peaks become broader with Al, Ni co-doped concentration which indicates a decrease in particle size. During doping process, some Al and Ni atoms may exist in the boundary of ZnO nanoparticles which reduces diffusion rate and crystal growth of ZnO. This process was also observed by previous literature of ZnO nanoparticles [55]. The average particles size was calculated by Debye-Scherrer equation [56]. The particle size, lattice parameters, FWHM and c/a ratio are given in Table1. The full width at half maximum (FWHM) of major diffraction peak (101) enhances with increase in Al, Ni co-doping dosage in ZnO. The average particle size for ZnO was found to be decreased with (Al, Ni) co-doping. This decrease in average particle size may be attributed to reduction in nucleation of ZnO nanoparticles by Al and Ni co-doping [90]. Also lattice constant 'a' was increased while c was decreased with increase in Al and Ni co-doping concentration ZnO. This may be due to stress formation induced by ionic radii difference of $Al^{+2}(0.54\text{\AA})$ and $Ni^{+2}(0.69\text{\AA})$ compared to that of $Zn^{+2}(0.74\text{\AA})$ [57].

Table 1. Lattice parameters and particle size of Al, Ni doped ZnO nanoparticles.

Samples Name	I_{max}	2θ	FWHM (β)	Particle size (nm)	Lattice Parameters		c/a ratio
					a(\AA)	c(\AA)	
X= 0%	6502	36.80	0.2047	42.73	3.262	5.212	1.598
X= 1%	6340	36.74	0.2065	42.36	3.271	5.195	1.588
X = 2%	5827	36.70	0.2109	41.47	3.285	5.189	1.580
X= 3%	5558	36.68	0.2134	40.98	3.287	5.187	1.578
X= 4%	5430	36.64	0.2167	40.35	3.294	5.183	1.573
X= 5%	5188	36.60	0.2218	39.42	3.298	5.178	1.570

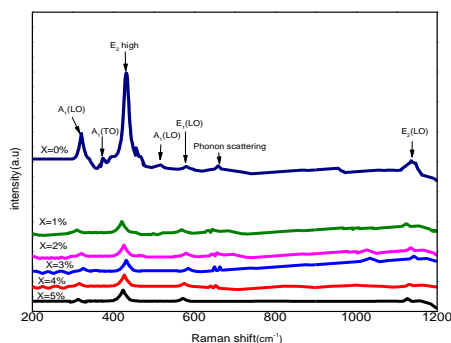


Fig.3. Raman spectra of ZnO and of $Al_xNi_xZnO_{1-2x}$ nanoparticles calcined at $700^\circ C$ for 3h.

3.2. Raman spectroscopy analysis

Raman spectroscopy is used to study oxygen bond vibrations, crystal phase defects and influence of dopants on vibrational modes. The Raman spectra of pure ZnO nanoparticles show bonds which are identical to wurtzite structure and in agreement with previous literature [58], while Raman spectroscopy of $Al_xNi_xZnO_{1-2x}$ nanoparticles enables to recognize Raman active mode characteristics of ZnO [59-61]. E_2 high mode at 433cm^{-1} was due to oxygen displacement in hexagonal wurtzite phase of ZnO and its intensity reduced rapidly with increase in (Al, Ni) doping as compared to ZnO. The peak at 322cm^{-1} was due to optical phonon over A_1 symmetry [62] and signal at 375cm^{-1} was due to A_1 transverse optical phonon [59] respectively. The Raman signals observed at 516cm^{-1} and 579cm^{-1} were attributed to $A_1(\text{LO})$ and $E_1(\text{LO})$ longitudinal optical phonon mode. These were associated with structural defects such as zinc interstitials, oxygen vacancies etc and their intensity enhanced with increase in (Al, Ni) doping concentration [63, 60]]. The signal observed at 600cm^{-1} was due to phonon scattering processes [58].

The Raman peak observed at 1134cm^{-1} was due to E_2 vibrational mode LO [60, 64]. It is clear from Raman spectra that as doping concentration increases up to 3%, the Raman frequencies become blue shifted due to decrease in particles size. At higher doping concentration, red shift in Raman frequency was observed due to tensile strain, heating and other effects like phonon confinement [55]. These evidences are in agreement with previous literature and prove that (Al, Ni) doping alters the basic hexagonal structure of ZnO and reduces the crystal symmetry and produce vacancies and substitutional defects.

3.3. SEM

Fig. 4 shows SEM images of pure ZnO and $Al_xNi_xZnO_{1-2x}$ samples. It can be seen that particles are irregular in shape. Also it shows that particles are randomly oriented and nearly spherical in shape, and agglomeration of nanoparticles is nearly restricted due to co-doping of (Al, Ni). This lowered agglomeration enhances photocatalytic performance due to additional active sites to adsorb molecules effectively. In addition to lower agglomeration, surface becomes scratchy due to existence of (Al, Ni) implying good dispersion of Al and Ni throughout the photocatalyst. Also observed high porosity may be due to liberation of gaseous products during combustion reaction.

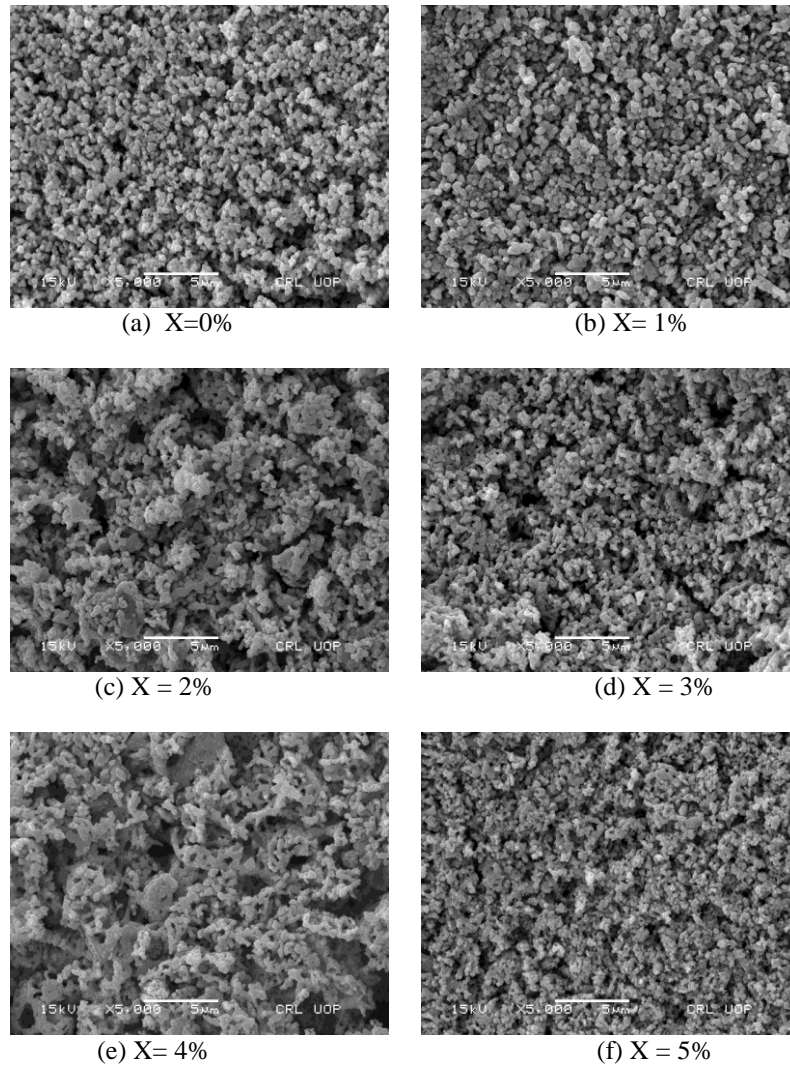


Fig.4. SEM images of ZnO and $Al_xNi_xZnO_{1-2x}$ nanoparticles.

3.4. Optical properties

UV-vis spectra

To study the optical properties of pure ZnO and $Al_xNi_xZnO_{1-2x}$ ($x= 0\%$, 1% , 2% , 3% , 4% , 5%) samples, UV-vis absorption spectra were measured at room temperature (figure 5). The electronic absorption spectrum showed a sharp absorption band at around 393 nm for ZnO sample. This absorption band may be attributed to wide band gap of ZnO and suggests that ZnO has limited light absorption ability [51]. The absorption edge was shifted towards larger wavelength with increase in (Al, Ni) doping concentration due to Al and Ni substitution affect into ZnO lattice. Al, Ni doped ZnO nanoparticles show stronger absorption in wavelength (300-500nm) due to surface modification and the light absorption increases due to enhancement in surface charge carrier transfer rate [65, 66]. The best photocatalytic efficiency was shown by $x=3\%$ (Al, Ni) doped ZnO sample in visible region which is in agreement with previous literature [67]. Thus photocatalytic activity was improved due to absorption shifting from UV region to visible region by co-doping of (Al, Ni) into ZnO sites.

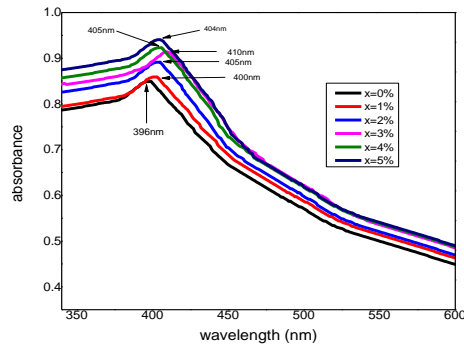


Fig. 5. UV-vis absorption spectra of Al, Ni doped ZnO nanoparticles.

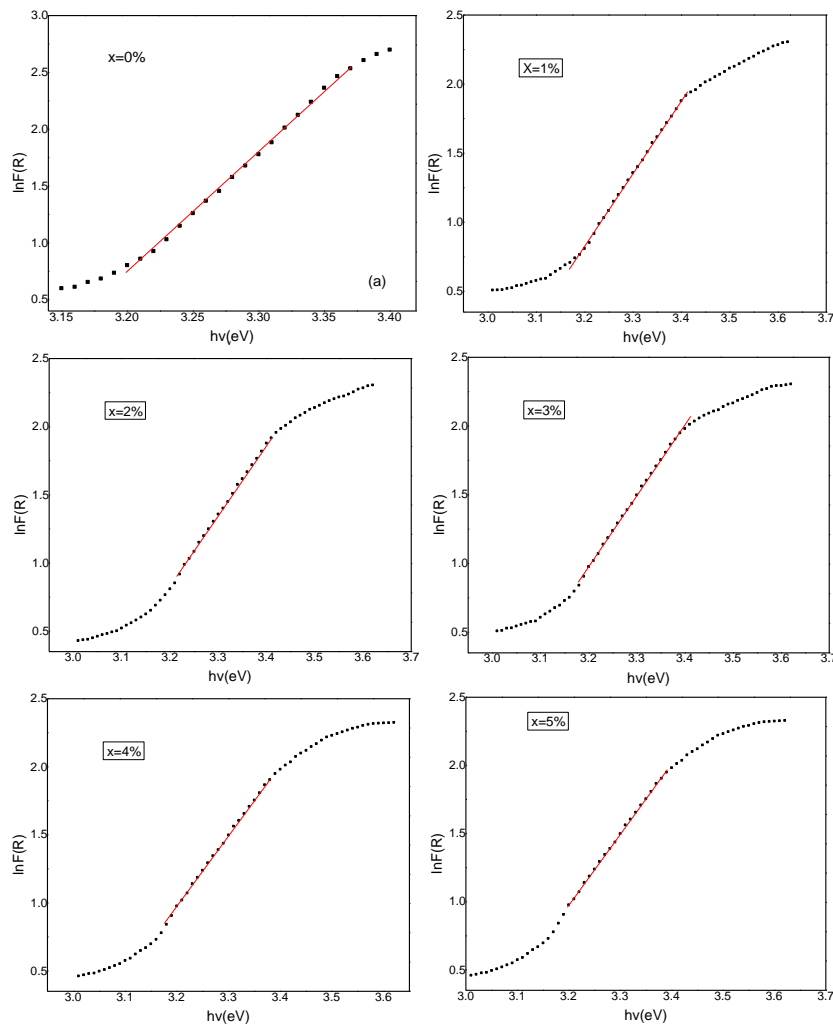


Fig. 7. Variation of $\ln F(R)$ versus $h\nu$ for Al, Ni doped ZnO samples.

The optical band gap of ZnO nanoparticles for different (Al, Ni) doping concentration was also measured. The band gap of (Al, Ni) doped ZnO nanoparticles was estimated from plot of $(\alpha h\nu)^2$ versus $h\nu$ in Fig. 7, here $h\nu$ is photon energy and α is absorption coefficient [68]. The optical band gap calculated for ZnO was found to be 3.31 eV while 3.30 eV, 3.28 eV, 3.27 eV, 3.29 eV, 3.30 eV for $\text{Al}_x\text{Ni}_x\text{ZnO}_{1-2x}$ ($x=0\%$, 1%, 2%, 3%, 4%, 5%) samples respectively. The optical band gap first decreased with (Al, Ni) co-doping and then increased with higher co-doping.

The minimum band gap was measured for $x=3\%$ (Al, Ni) doped ZnO nanoparticles and similar band shift has been reported by many researchers [69-71].

3.5. PL analysis

Charge separation property of the photocatalyst is measured by PL analysis [72-73]. PL intensity is directly related to electron hole recombination rate [74,65]. So more intense peak of photocatalyst means to possess higher intensity and higher electron hole pair rate, which is big hindrance to photocatalytic performance [74]. It can be seen that pure ZnO has more intense peaks than other samples, suggesting ZnO has larger electron hole recombination rate which suppresses the photocatalytic performance of ZnO. The emission intensity reduces with doping concentration because dopants capture the charge carriers through the interface to produce the charge separation [65, 66, 75]. The synthesized samples showed three emission bands: band edge emission at 390nm, violet emission at 422 nm, blue emission at 454nm, blue green emission at 474nm and green emission at 531nm respectively. The UV emission observed at 390 was due to free excitons recombination (electron hole pair) from conduction band and valence band [76]. Various intrinsic defects in ZnO such as oxygen antisites (O_{zn}), oxygen vacancies (V_o), oxygen interstitials (O_i), zinc interstitials (Zn_i) and zinc vacancies (V_{zn}) caused visible emission [77-79]. Violet emission was observed due to electron transition from valence band edge to shallow level of neutral zinc (Zn_i) [78-79]. Blue emission was observed due to electronic transition from shallow donor level of neutral Zn_i to an acceptor level of neutral V_{zn} [80]. Blue green emission was observed due to energy gap between valence band edge and donor level of Zn_i [81-82], while green emission was attributed to electronic transition between valence band edge and oxygen vacancies level [83]. It can be seen that $x=3\%$ Al, Ni doped ZnO has the lowest intensity and minimum electron hole pair rate. So $x=3\%$ Al, Ni doped ZnO exhibited best photocatalytic performance. Increase in intensity for higher doping reduced the photocatalytic activity which is in agreement in previous studies.

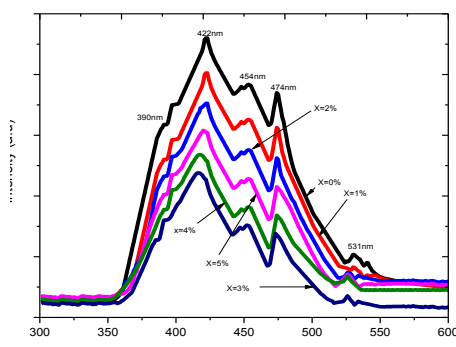


Fig. 8. PL spectra of $Al_xNi_xZnO_{1-2x}$ nanoparticles.

3.6 Photocatalytic activity

Lactic acid (LA) solution was used to investigate photocatalytic hydrogen production of synthesized $Al_xNi_xZnO_{1-2x}$ nanoparticles. A 300 Xe arc lamp with cut off filter was used for visible light irradiation. LA did not show any photocatalytic hydrogen production in deficiency of photocatalyst and under no light irradiation [84]. Then 0.05 g of photocatalyst was dispersed in LA and irradiated by arc lamp. It can be seen from the figure that pure ZnO showed least hydrogen production among all prepared samples. The reason behind this may be very minute light absorption capability of ZnO nanoparticles and fast electron hole pair rate [73]. $Al_xNi_xZnO_{1-2x}$ ($x=1\%$) sample shows higher photocatalytic than pure ZnO because incorporation of Al dopants can speed up division and lowers electron hole pair rate [65-66]. Also Ni plays a role of co-catalyst which assists photocatalytic behavior through photoelectron excitation at boundary sites of ZnO nanoparticles [65-66, 85]. The photocatalytic hydrogen production increases up to $Al_xNi_xZnO_{1-2x}$ ($x=3\%$) nanoparticles. This improvement in photocatalytic hydrogen production was observed due to creation of vacancies at the surface and grain boundaries of ZnO. The existence of oxygen vacancies reduces further formation of nanoparticles and produces a stress field. The oxygen

vacancy will play the role of scattering centre for charge carriers and will evade electron hole pair rate. This results in improvement of photocatalytic behavior [86]. Al and Ni doping exhibited positive synergetic effect on photocatalytic activity of ZnO nanoparticles. This may be due to formation of impurity levels above valence band due to addition of Al and Ni ions into ZnO lattice, which alters light absorption response from UV region to visible region. So it reduces band gap energy of ZnO nanoparticles, resulting in creation of more photo generated electrons and holes which participates in photocatalytic activity. Also dopant reduces electron hole pair recombination rate and Al and Ni existing on the surface of ZnO improves photocatalytic activity. Higher doping (x=4%, 5%) leads to reduction of photocatalytic hydrogen production. This may be due to covering of ZnO surface by excess Al and Ni particles [55]. Therefore light absorption ability of the photocatalyst is reduced and few photocatalyst sites can be stimulated. Also higher doping of Al and Ni reduces the surface area due to agglomeration of nanoparticles [87-88]. The quantity of hydrogen produced under light irradiation ($\lambda = 410\text{nm}$) in one hour was used to calculate quantum efficiency.

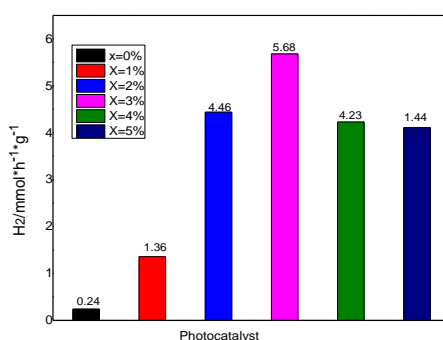


Fig. 9. Photocatalytic hydrogen production performance of as synthesized $\text{Al}_x\text{Ni}_x\text{ZnO}_{1-2x}$ photocatalysts.

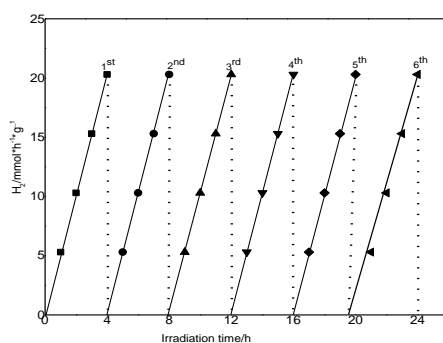


Fig. 10. Long term hydrogen evolution performance of Al, Ni doped ZnO (x=3%) photocatalyst under visible light irradiation for 24 hours.

Table 2. Hydrogen evolution rate and quantum efficiency of as synthesized photocatalysts.

Sample	$\text{H}_2/\text{mmol}\cdot\text{h}^{-1}\cdot\text{g}^{-1}$	QE/%
X=0%	0.24	0.9
X= 1%	1.36	1.21
X= 2%	4.46	1.26
X= 3%	5.68	2.15
X= 4%	4.23	1.64
X= 5%	4.11	1.47

From Table 2 it can be seen that $x=3\%$ sample showed maximum apparent quantum efficiency of 2.15% at 410 nm among all prepared photocatalysts. Also QE was 0.9% for $x=0\%$ sample, 1.26% for $x=1\%$ sample, 1.26% for $x=2\%$ sample, 1.47% for $x=4\%$ sample and 1.64% for $x=5\%$ sample respectively.

4. Conclusion

Al and Ni co-doped ZnO and pure ZnO nanoparticles have been successfully prepared via combustion method. The structural, morphological and optical properties exhibited successful synthesis of $\text{Al}_x\text{Ni}_x\text{ZnO}_{1-2x}$ nanoparticles. Al, Ni co-doped ZnO samples showed extended visible light absorption and lower electron hole pair recombination rate. The photocatalytic activity of the prepared samples was measured in aqueous solution containing lactic acid under visible light irradiation. The best photocatalytic hydrogen production activity was observed for ($X=3\%$) photocatalyst. It is observed that enhancing Al, Ni doping concentration leads to a reduction in photocatalytic hydrogen production. Consequently, Al, Ni co-doped ZnO nanoparticles photocatalyst have proven potential candidacy for photocatalytic hydrogen evolution applications.

References

- [1] N.R.Khalid, Z. Hong, E.Ahmed, Y.Zhang, H.Chan, M.Ahmad, Applied Surface Science **258**(15), 5827 (2012).
- [2] M.Li, Z.Hong, Y.Fang, F.Huang, Materials Research Bulletin **43**(8-9), 2179 (2008).
- [3] K.Naeem, F. Ouyang, Physica B: Condensed Matter **405**(1), 221 (2010).
- [4] Y.Xu, B.Lei, L. Guo, W.Zhou, Y.Liu, Journal of Hazardous Materials **160**(1), 78 (2008).
- [5] C.Chen, W.Ma, J.Zhao, Current Organic Chemistry **14**(7), 630 (2010).
- [6] H.H.Tseng, M.C.Weil, S.F. Hsiung, C.W.Chiou, Chemical Engineering Journal **150**(1), 160 (2009).
- [7] T.C.Zhang, Z.X.Mei, Y.Guo, Q.K. Xue, X.L.Du, Journal of Physics D: Applied Physics **42**(11), 119801 (2009).
- [8] Z.L.S.Seow, A.S.W.Wong, V.Thavasi, R.Jose, S. Ramakrishna, G.W. Ho, Nanotechnology **20**(4), 045604 (2008).
- [9] C.Y.Jiang, X.W.Sun, G.Q.Lo, D.L. Kwong, J.X.Wang, Applied Physics Letters **90**(26), 263501 (2007).
- [10] A.Tripathi, K.P. Misra, R.K. Shukla, Journal of Luminescence **149**, 361 (2014).
- [11] Z.F.Liu, F.K.Shan, J.Y.Sohn, S.C. Kim, G.Y. Kim, Y.X.Li, Journal of Electroceramics **13**(1-3), 183 (2004).
- [12] R.Wang, J.H.Xin, Y. Yang, H.Liu, L.Xu, J.Hu, Applied Surface Science **227**(1-4), 312 (2004).
- [13] W.Park, T.C. Jones, C.J.Summers, Applied Physics Letters **74**(13), 1785 (1999).
- [14] E.Burunkaya, N.Kiraz, Ö.Kesmez, H.E.Camurlu, M.Asiltürk, E.Arpaç, Journal of Sol-Gel Science and Technology **55**(2), 171 (2010).
- [15] S.H.Park, J.B. Park, P.K. Song, Current Applied Physics **10**(3), S488 (2010).
- [16] X.Liu, L.Pan, Q.Zhao, T.Lv, G. Zhu, T.Chen, T.Lu, Z. Sun, C.Sun, Chemical Engineering Journal **183**, 238 (2012).
- [17] S.Liu, H.Sun, A.Suvorova, S.Wang, Chemical Engineering Journal **229**, 533 (2013).
- [18] L.Ling, S.Zhao, P.Han, B.Wang, R.Zhang, M.Fan, Chemical Engineering Journal **244**, 364 (2014).
- [19] M.Ahmad, E.Ahmed, Y. Zhang, N.R.Khalid, J.Xu, M.Ullah, Z.Hong, Current Applied Physics **13**(4), 697 (2013).
- [20] M.Li, Z.Hong, Y.Fang, F. Huang, Materials Research Bulletin **43**(8-9), 2179 (2008).
- [21] M.Li, P.Tang, Z.Hong, M.Wang, Colloids and Surfaces A: Physicochemical and Engineering Aspects **318**(1-3), 285 (2008).
- [22] S.F.Zhou, Z.L. Hong, F.R.Zhao, X.P. Fan, M.Q.Wang, Journal of Inorganic Materials **4**,

- 03 (2006).
- [23] M.Samadi, M.Zirak, A.Naseri, E. Khorashadizade, A.Z.Moshfegh, *Thin Solid Films* **605**, 2 (2016).
- [24] M.Shakir, M.Faraz, M.A. Sherwani, S.I.Al-Resayes, *Journal of Luminescence* **176**, 159 (2016).
- [25] D.Wang, H.Liu, Y.Ma, J.Qu, J.Guan, N.Lu, Y. Lu, X.Yuan, *Journal of Alloys and Compounds* **680**, 500 (2016).
- [26] R.Velmurugan, M.Swaminathan, *Solar Energy Materials and Solar Cells* **95**(3), 942 (2011).
- [27] C.Yu, K.Yang, Y.Xie, Q.Fan, C.Y.Jimmy, Q. Shu, C.Wang, *Nanoscale* **5**(5), 2142 (2013).
- [28] Y.H.Leung, X.Y.Chen, A.Ng, M.Y.Guo, F.Z.Liu, A.B.Djurišić, W.K.Chan, X.Q. Shi, M.A. Van Hove, *Applied Surface Science* **271**, 202 (2013).
- [29] B.M. Rajbongshi, S.K.Samdarshi, *Applied Catalysis B: Environmental* **144**, 435 (2014).
- [30] K.G.Kanade, B.B. Kale, J.O.Baeg, S.M.Lee, C.W.Lee, S.J. Moon, H.Chang, *Materials Chemistry and Physics* **102**(1), 98 (2007)
- [31] R.Kumar, A.Umar, G.Kumar, M.S.Akhtar, Y. Wang, S.H. Kim, *Ceramics International* **41**(6), 7773 (2015).
- [32] F.Achouri, S.Corbel, L.Balan, K.Mozet, E.Girot, G.Medjahdi, M.B. Said, A.Ghrabi, R. Schneider, *Materials & Design* **101**, 309 (2016).
- [33] R.C.Pawar, D.H.Choi, J.S. Lee, C.S.Lee, *Materials Chemistry and Physics* **151**, 167 (2015).
- [34] C.Abed, C.Bouzidi, H.Elhouichet, B. Gelloz, M.Ferid, *Applied Surface Science* **349**, 855 (2015).
- [35] H.J.Lee, J.H.Kim, S.S.Park, S.S. Hong, G.D.Lee, *Journal of Industrial and Engineering Chemistry* **25**, 199 (2015).
- [36] O.Saber, T.A. El-Brolossy, A.A.Al Jaafari, *Water, Air, & Soil Pollution* **223**(7), 4615 (2012).
- [37] X.Li, Z.Hu, J.Liu, D.Li, X.Zhang, J. Chen, J.Fang, *Applied Catalysis B: Environmental* **195**, 29 (2016).
- [38] H.J.Lee, J.H.Kim, S.S.Park, S.S. Hong, G.D.Lee, *Journal of Industrial and Engineering Chemistry* **25**, 199 (2015).
- [39] M.Ahmad, E.Ahmed, Y.Zhang, N.R.Khalid, J.Xu, M.Ullah, Z.Hong, *Current Applied Physics* **13**(4), 697 (2013).
- [40] O.Saber, T.A. El-Brolossy, A.A. Al Jaafari, *Water, Air, & Soil Pollution* **223**(7), 4615 (2012).
- [41] M.Ahmad, E.Ahmed, Y.Zhang, N.R.Khalid, J.Xu, M. Ullah, Z.Hong, *Current Applied Physics* **13**(4), 697 (2013).
- [42] K.C.Barick, S.Singh, M.Asalam, D.Bahadur, *Microporous and Mesoporous Materials* **134**(1-3), 195 (2010).
- [43] J.Zhao, L.Wang, X.Yan, Y.Yang, Y.Lei, J.Zhou, Y.Huang, Y.Gu, Y.Zhang, *Materials Research Bulletin* **46**(8), 1207 (2011).
- [44] N.Hasuike, R.Deguchi, H.Katoh, K.Kisoda, K.Nishio, T. Isshiki, H.Harima, *Journal of Physics: Condensed Matter* **19**(36), 365223 (2007).
- [45] K.C.Barick, S.Singh, M.Asalam, D. Bahadur, *Microporous and Mesoporous Materials* **134**(1-3), 195 (2010).
- [46] B.Subash, B.Krishnakumar, R.Velmurugan, M.Swaminathan, M.Shanthi, *Catalysis Science & Technology* **2**(11), 2319 (2012).
- [47] X.Wang, G.Li, Y.Wang, *Chemical Physics Letters* **469**(4-6), 308 (2009).
- [48] Q.I.Li, N.J. Easter, J.K.Shang, *Environmental Science & Technology* **43**(5), 1534 (2009).
- [49] X.Yang, F. Ma, K.Li, Y.Guo, J.Hu, W. Li, M.Huo, Y.Guo, *Journal of Hazardous Materials* **175**(1-3), 429 (2010).
- [50] Q.Hu, C.Wu, L.Cao, B.Chi, J.Pu, L. Jian, *Journal of Power Sources* **226**, 8 (2013).
- [51] J.Huo, L. Fang, Y.Lei, G.Zeng, H.Zeng, *Journal of Materials Chemistry A* **2**(29), 11040 (2014).
- [52] D.Zhang, J.Gong, J.Ma, G. Han, Z.Tong, *Dalton Transactions* **42**(47), 16556 (2013).

- [53] J. Alaria, M. Venkatesan, J.M.D. Coey, *Journal of Applied Physics* **103**(7), 07D123 (2008).
- [54] J. Zhao, L. Wang, X. Yan, Y. Yang, Y. Lei, J. Zhou, Y. Huang, Y. Gu, Y. Zhang, *Materials Research Bulletin* **46**(8), 1207 (2011).
- [55] I.N.Reddy, C.V.Reddy, J.Shim, B.Akkinpally, M.Cho, K. Yoo, D.Kim, *Catalysis Today* 2018.
- [56] A.Senthilraja, B.Subash, B.Krishnakumar,D.Rajamanickam,M.Swaminathan, M.Shanthi, *Materials Science in Semiconductor Processing* **22**,83 (2014).
- [57] A.Bedia, F.Z.Bedia, M. Aillerie, N.Maloufi, *Superlattices and Microstructures* **111**, 714 (2017).
- [58] J.M. Calleja, M.Cardona,*Physical Review B* **16**(8), 3753 (1977).
- [59] A.K.Ojha,M. Srivastava, S.Kumar, R.Hassanein, J.Singh, M.K. Singh, A.Materny, *Vibrational Spectroscopy* **72**, 90 (2014).
- [60] J.Das, S.K.Pradhan, D.R.Sahu, D.K.Mishra,S.N. Sarangi, B.B.Nayak, S.Verma, B.K. Roul, *Physica B: Condensed Matter* **405**(10), 2492 (2010).
- [61] R.Cuscó, E.Alarcón-Lladó, J.Ibanez, L.Artús, J.Jimenez, B. Wang, M.J.Callahan, *Physical Review B* **75**(16), 165202 (2007).
- [62] R.Zhang, P.G. Yin, N. Wang, L.Guo,*Solid State Sciences* **11**(4), 865 (2009).
- [63] I.Lorite, L.Villaseca, P.Díaz-Carrasco, M.Gabás, J.L.Costa-Krämer,*Thin Solid Films***548**, 657 (2013).
- [64] B.Hadžić,N.Romčević, M.Romčević, I.Kuryliszyn-Kudelska, W.Dobrowolski, R.Wróbel, U.Narkiewicz, D.Sibera,*Journal of Alloys and Compounds* **585**,214 (2014).
- [65] C.Y.Su, C.T.Lu, W.T.Hsiao, W.H.Liu, F.S.Shieu, *Thin Solid Film* **544**, 170 (2013).
- [66] Z.Zhan, Y.Wang, Z.Lin, J. Zhang, F.Huang, *Chemical Communications* **47**(15), 4517 (2011).
- [67] J.Huo, L.Fang, Y.Lei, G.Zeng, H.Zeng, *Journal of Materials Chemistry A* **2**(29), 11040 (2014).
- [68] X.M.Fan, J.S.Lian, Z.X. Guo, H.J.Lu, *Applied Surface Science* **239**(2), 176 (2005).
- [69] I.N. Reddy, C.V.Reddy,J. Shim, B.Akkinpally, M.Cho, K. Yoo, D.Kim, *Catalysis Today*2018.
- [70] I.Ganesh, *Ceramics International* **42**(8), 10410 (2016).
- [71] S.Bhatia, N. Verma, R.K.Bedi, *Materials Research Bulletin* **88**, 14 (2017).
- [72] S.Usai, S.Obregón, A.I. Becerro, G.Colón, *The Journal of Physical Chemistry C* **117**(46), 24479 (2013).
- [73] M.Salavati-Niasari, F.Davar, A.Khansari, *Journal of Alloys and Compounds* **509**(1), 61 (2011).
- [74] S.Martha, K.H. Reddy, K.M.Parida,*Journal of Materials Chemistry A* **2**(10), 3621 (2014).
- [75] Z.Hamden,D.P. Ferreira, L.V. Ferreira,S.Bouattour, *Ceramics International* **40**(2), 3227 (2014).
- [76] D. Theyvaraju, S.Muthukumaran, *Physica E: Low-dimensional Systems and Nanostructures* **74**, 93 (2015).
- [77] P.Li, S.Wang, J.Li, Y.Wei, *Journal of Luminescence* **132**(1), 220 (2012).
- [78] A.S.Kumar, N.M. Huang, H.S.Nagaraja, *Electronic Materials Letters* **10**(4), 753 (2014).
- [79] S.K.Mishra, S. Bayan, R.Shankar, P.Chakraborty, R.K.Srivastava,*Sensors and Actuators A: Physical* **211**, 8 (2014).
- [80] D.Raoufi, *Journal of Luminescence* **134**, 213 (2013).
- [81] D.H.Zhang, Q.P. Wang, Z.Y.Xue,*Applied Surface Science* **207**(1-4), 20 (2003).
- [82] G.H.Mhlongo, D.E.Motaung, S.S.Nkosi, H.C.Swart, G.F.Malgas, K.T. Hillie, B.W. Mwakikunga, *Applied Surface Science* **293**, 62 (2014).
- [83] K.Vanheusden, W.L.Warren, C.H.Seager, D.R.Tallant, J.A. Voigt,B.E.Gnade, *Journal of Applied Physics* **79**(10), 7983 (1996).
- [84] F.Wen, C.Li,*Accounts of Chemical Research* **46**(11), 2355 (2013).
- [85]J.Huo, L.Fang, Y.Lei, G. Zeng, H.Zeng, *Journal of Materials Chemistry A* **2**(29), 11040 (2014).
- [86] U.Alam,A. Khan,W. Raza, A.Khan, D. Bahnemann, M.Muneer,*Catalysis Today* **284**, 169 (2017).

- [87] A.N.Rao, B.Sivasankar, V.Sadasivam, *Journal of Molecular Catalysis A: Chemical* **306**(1-2), 77 (2009).
- [88] P. Bansal, D.Sud, *Desalination* **267**(2-3), 244 (2011).
- [89] B.Subash, B.Krishnakumar, M. Swaminathan, M.Shanthi, *Langmuir* **29**(3), 939 (2013).
- [90] N.F.Djaja, D.A. Montja, R. Saleh, *Advances in Materials Physics and Chemistry* **3**(01), 33 (2013).